Unblowing bubbles: understanding the physics of bubble deflation through a straw

Daniele Battesimo Provenzano[(a)], Andrea Stefanini[(b)]

[(a)] Scuola Normale Superiore, Pisa, Italia — daniele.provenzano@sns.it

[(b)] I.T.I.S. "Galileo Galilei", Livorno, Italia — andrea.stefanini@aif-fisica.org

(Dated: July 23, 2025)

A formal description of the deflation process of a soap bubble attached to a cylindrical tube is provided, with emphasis on quantifying viscous and unsteady effects. Differing from prior studies, the proposed theoretical framework maintains its validity across a wide spectrum of parameter values that define the system. The model is validated through experimental results that can be reproduced at home using liquid soap and a straw, emphasizing its educational aspects.

I. INTRODUCTION

Soap bubbles have been used for centuries to entertain and enchant children. They are held together by surface tension, which causes the pressure of the air inside to be larger than the atmospheric pressure. This difference in pressure causes bubbles to deflate when a hole is made on their surface, similar to unknotted party balloons. This phenomenon can be observed when trying to blow soap bubbles using an ordinary straw: if the inflated bubble does not detach from the straw, it will start deflating as soon as lips are removed from the other end.

The problem of a bubble deflating through a thin cylindrical tube was first introduced in Ref. 1 and was further explored in Ref. 2. In both works, the authors find that the deflation time is proportional to the fourth power of the initial radius of the bubble and to the length L of the tube. This result implies that the deflation time for a bubble attached to an infinitely short tube is null. This issue is not just a mere abstract fact, but also has experimental implications: a fairly thin ring constitutes precisely the limit $L \to 0$ of a tube. In this case, the results of Refs. 1 and 2 are not so useful, as will be shown in this work. On the other hand, they may constitute a good approximation if L is large enough. In this work, the limit case $L \to 0$ will be part of a broader class of cases, which will be referred to as the *inviscid* case and distinguished from the *viscous* one. The main purpose of this analysis is to derive and validate a more general model that works regardless of the value of L, as well as all other parameters.

The configuration under consideration is characterized by the following parameters:

- R_0, the initial radius of the bubble;
- L, the length of the straw;
- r_{straw}, the cross-sectional radius of the straw;
- $A = \pi r_{\text{straw}}^2$, the cross section of the straw;
- ρ, the density of air;
- μ, the viscosity of air;
- σ, the surface tension of soap.

For the remaining physical quantities, $R(t)$ is the instantaneous radius of the bubble, while v_i and p_i are the velocity and pressure of air at some point i in space.

Referring to Fig. 1, Bernoulli's equation will be used to link quantities inside the bubble - points 1 or 3 - to quantities just outside the straw - point 4. The correct application of Bernoulli's equation dictates some of this model's assumptions. Bernoulli's equation will appear in three different versions in the analysis, and distinct names will be assigned to each form in order to avoid confusion. The least general form of the equation—that is, the one requiring the most assumptions—will be referred to as the *Restricted Bernoulli's Equation* (RBE), and is written as:

$$p(\vec{r}) + \frac{1}{2}\rho v^2(\vec{r}) + \rho g z = \text{const.} \tag{1}$$

which holds under the assumptions of irrotational, steady and laminar flow in an inviscid and incompressible fluid.* The generalization of Eq. (1) to viscous fluids will be referred to as the *Viscous Bernoulli's Equation* (VBE). Finally, when unsteady effects will be incorporated into the VBE in Sec. IV, it will be referred to as the *Unsteady Viscous Bernoulli's Equation* (UVBE).

Air will be assumed to be incompressible throughout the entire work. This assumption is justified by the fact that the highest velocity in the system is two orders of magnitude smaller than the speed of sound. Hence, the continuity equation reads

$$-4\pi R^2(t)\,\frac{\mathrm{d}R}{\mathrm{d}t} = A\,v_S(t), \tag{2}$$

where $v_S(t) = v_3 = v_4$ is the homogeneous velocity of air inside the straw. It is important to note that $v_S(t)$ is homogeneous throughout the cross section of the straw only if $\mu \to 0$. Hence, when viscous effects cannot be neglected, $v_S(t)$ will represent the average velocity on the cross section. As for the velocity inside the bubble,

* If the assumption of irrotationality alone does not hold, the validity of Eq. (1) is restricted to a single streamline rather than the entire flow.

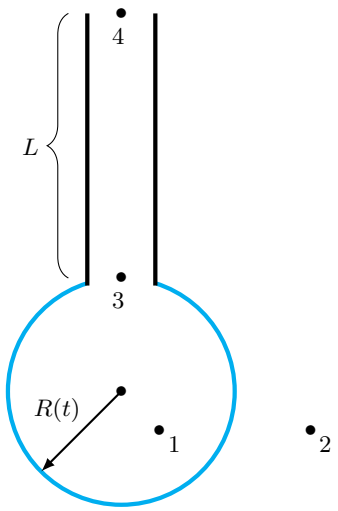

FIG. 1. Schematization of the bubble-straw system.

it will be assumed to be negligibly small. The validity of this assumption will be analyzed in Sec. IV.

The last fundamental assumption of this model concerns the shape of the bubble, which will be assumed to be spherical. Of course, this assumption is broken when the radius of the bubble becomes comparable to the radius of the straw.[2] However, the correction to the total deflation time is negligible, as will be shown in Sec. III.

Finally, it should be noted that the result depends neither on the acceleration of gravity g nor on the inclination of the straw. This feature can be explained by means of Archimedes' law: no work needs to be done to move up a volume of fluid inside a larger volume of the same fluid.[†] For the same reason, the deflation time is the same for vertical and horizontal straws, assuming that all other quantities are kept fixed. The same holds true when viscous and unsteady effects are taken into account. Thus, referring to Fig. 1, the RBE, relating quantities in points 1 and 4, simply reads

$$\frac{4\sigma}{R(t)} + \frac{1}{2}\rho v_1^2 = \frac{1}{2}\rho v_4^2, \tag{5}$$

where

$$\frac{4\sigma}{R(t)} = p_1 - p_2 \tag{6}$$

is the pressure difference due to the Young–Laplace equation.[3]

II. THEORETICAL MODELS

Before delving into analytical calculations, it is worth saying something about the relationship between quantities that characterize the system. Through the use of dimensional analysis, specifically the Buckingham π theorem and the principle of similitude,[4, 5] it is possible to find how the deflation time depends on the other quantities. In the case where viscous effects are negligible, it is reasonable to assume that the deflation time only depends on R_0, A, σ and ρ. Using the tools aforementioned, the functional relation one finds is

$$t_I = \sqrt{\frac{\rho}{\sigma}}\, R_0^{3/2}\, \mathcal{F}\left(\frac{R_0^2}{A}\right), \tag{7}$$

where the subscript I refers to the *inviscid* case and $\mathcal{F}(x)$ is a generic real-valued function.

In contrast, if viscous effects are not negligible, it is reasonable to assume that the deflation time depends on R_0, A, σ, L and μ. It does not depend on the density ρ because, in the viscous regime, most of the energy stored on the surface of the bubble is dissipated in the straw by viscous forces, which do not carry any information about the density. Under such assumptions, one gets

$$t_V = \frac{\mu}{\sigma}\, R_0\, \mathcal{G}\left(\frac{R_0^2}{A}, \frac{L}{R_0}\right), \tag{8}$$

where the subscript V refers to the *viscous* case and $\mathcal{G}(x, y)$ is a generic real-valued function. The results of the upcoming analysis must respect Eqs. (7) and (8).

The inviscid case is determined by the solution of Eqs. (2) and (5). Assuming the air velocity inside the bubble is negligible, as it is in the initial moments of deflation, the system of equations reduces to

$$4\pi R^2(t)\,\frac{\mathrm{d}R}{\mathrm{d}t} = -A\sqrt{\frac{8\sigma}{\rho R(t)}}. \tag{9}$$

Separating variables and integrating leads to

$$R(t) = \left(R_0^{7/2} - \frac{7\sqrt{2}\,A}{4\pi}\sqrt{\frac{\sigma}{\rho}}\,t\right)^{2/7}, \tag{10}$$

---

† The mathematical justification proceeds as follows. Referring to Fig. 1, the RBE is applied between points 1 and 4, under the assumption of inviscid air:

$$p_1 + \frac{1}{2}\rho v_1^2 + \rho g z_1 = p_4 + \frac{1}{2}\rho v_4^2 + \rho g z_4, \tag{3}$$

where z_i denotes the vertical coordinate. Given that $z_4 - z_1 \approx L$, and using the Young–Laplace law $p_1 = p_2 + \frac{4\sigma}{R(t)}$, along with Stevin's law $p_2 = p_4 + \rho g(z_4 - z_2) \approx p_4 + \rho g L$, the equation reduces to

$$\frac{4\sigma}{R(t)} + \frac{1}{2}\rho v_1^2 = \frac{1}{2}\rho v_4^2, \tag{4}$$

which shows that the dependence on g cancels out. This outcome is consistent with physical intuition: in the absence of the bubble, no airflow would occur, i.e., $v_1 = v_4 = 0$. Indeed, even in a very long vertical tube in open air, no flow is observed despite the presence of a pressure difference between the top and bottom ends, due to Stevin's law. The same result holds when viscous and unsteady effects are taken into account, because the terms $p(\vec{r})$ and $\rho g z$ remain unchanged.

which implies the following expression for the deflation time

$$t_{\mathrm{I}} = \frac{4\pi R_0^{7/2}}{7\sqrt{2}\,A}\sqrt{\frac{\rho}{\sigma}}. \tag{11}$$

It can be seen that Eq. (11) respects Eq. (7) with $\mathcal{F}(x) = 4\pi x/7\sqrt{2}$.

If viscous effects are not negligible, the RBE can no longer be applied. In this case, a suitable replacement is Poiseuille's law,[6] which in this context reads:

$$p_3 - p_4 - \rho g L = \frac{8\pi\mu L Q(t)}{A^2}, \tag{12}$$

where $Q(t) = A\,v_S(t)$ is the volumetric flow rate of air in the straw. Equation (12) reduces to

$$\frac{4\sigma}{R(t)} = \frac{8\pi\mu L}{A}\,v_S(t). \tag{13}$$

As stated previously, in this case $v_S(t)$ represents the average velocity of air over the entire cross section. Solving Eqs. (2) and (13), one finds

$$R(t) = \left(R_0^4 - \frac{\sigma A^2}{2\pi^2\mu\,L}\,t\right)^{1/4}, \tag{14}$$

Hence, the deflation time is

$$t_V = \frac{2\pi^2\mu\,L R_0^4}{\sigma A^2}, \tag{15}$$

which respects Eq. (8) with $\mathcal{G}(x,y) = 2\pi^2\,x^2 y$. The viscous model described by Eqs. (14) and (15) was used in Refs. 1 and 2.

In summary, the deflation time is proportional to $R_0^{7/2}$ in the inviscid model, while it is proportional to R_0^4 in the viscous one. A difference in the functional dependencies suggests that a more general expression for the deflation time should exist.

The fundamental difference between the previous models lies in the mechanism that prevents air from escaping the bubble instantaneously. The inviscid model accounts only for inertia, whereas the viscous model considers only viscosity.[‡] As a result, the inviscid model remains unaffected by the length of the straw, while the viscous model does depend on it. Specifically, as $L \to 0$, while keeping the other parameters fixed, the viscous model predicts $t_V \to 0$, whereas the inviscid model always yields a constant deflation time. This is consistent with expectations, as air inertia ensures a nonzero deflation time even when a small hole is punctured in the bubble.[§]

A third, more comprehensive model should incorporate both inertia and viscosity, correctly converging to the expected limiting behavior for both long, thin straws and short, wide straws. The aim of the final part of this section is to find a more general approach to the problem, which unifies the RBE and the concept of viscosity. The most natural way of doing so is to generalize Bernoulli's equation to viscous fluids, thus writing the *Viscous Bernoulli's Equation* (VBE) as done in Ref. 8.[¶] By applying it between points 1 and 4, one obtains:

$$\frac{4\sigma}{R} = \frac{1}{2}\rho\,v_S^2 + \Delta p_{\mathrm{visc}}, \tag{16}$$

where Δp_{visc} is the pressure drop due to viscosity, given by Eq. (12). A qualitative justification for the presence of this term lies in the fact that the pressure difference between the two ends—namely, the quantity on the left-hand side—is partially converted into kinetic energy density and partially into energy density dissipated due to viscosity. For a more detailed discussion, see Ref. 8, specifically Section F, which addresses a more general case than the one considered here. Equation (16) reads

$$\frac{4\sigma}{R} = \frac{1}{2}\rho\,v_S^2 + \frac{8\pi\mu L}{A}\,v_S, \tag{17}$$

whose only physical solution is

$$v_S(R) = \sqrt{\left(\frac{8\pi\mu L}{\rho A}\right)^2 + \frac{8\sigma}{\rho R}} - \frac{8\pi\mu L}{\rho A}. \tag{18}$$

Inspection of Eq. (18) suggests factoring out a common term and introducing the dimensionless coefficient

$$\gamma = \frac{\sigma\rho A^2}{8\pi^2\mu^2 L^2 R} = \frac{\sigma\rho}{8\mu^2}\frac{r_{\mathrm{straw}}^4}{L^2 R}, \tag{19}$$

which can also be expressed as the ratio of two characteristic lengths of the system: a purely geometric one, $\Lambda \equiv r_{\mathrm{straw}}^4/L^2R$, and a material-dependent one, $\lambda \equiv 8\mu^2/\sigma\rho$, which in the present case is on the order of 100 nm. Note that both Λ and γ increase monotonically with time, as the bubble progressively shrinks. Hence, Eq. (18) can be written as

$$v_S = \frac{8\pi\mu L}{\rho A}\left(\sqrt{1+\gamma} - 1\right). \tag{20}$$

[‡] Indeed, in the inviscid model, the outflow velocity is inversely proportional to the square root of the air density, which represents its inertia. In contrast, the purely viscous model predicts an outflow velocity that is inversely proportional to the air viscosity.

[§] A slight variation of this scenario was analyzed in Ref. 7.

[¶] In Ref. 8 the authors highlight a common misconception in fluid dynamics: Bernoulli's equation and Poiseuille's law are often regarded as mutually exclusive. However, this view depends on which form of Bernoulli's equation is being considered. While the statement holds true for the RBE, it does not apply to its more general forms. In fact, the RBE and Poiseuille's law can be seen as two limiting cases of a more general relation, which is the *Viscous Bernoulli's Equation* (VBE). When the viscosity $\mu \to 0$, the general equation reduces to the RBE. Conversely, when the kinetic term $\rho v^2/2$ is negligible, it reduces to Poiseuille's law.

As will be evident shortly, it is convenient to rewrite Eqs. (11) and (15) by making use of the definition provided in Eq. (19). A simple substitution yields:

$$t_I = \frac{\rho R_0^3}{7\mu L}\,\gamma_0^{-1/2}, \tag{21}$$

$$t_V = \frac{\rho R_0^3}{4\mu L}\,\gamma_0^{-1}, \tag{22}$$

where $\gamma_0 \equiv \gamma(R = R_0) \equiv \gamma(t = 0)$. Substituting Eq. (18) in Eq. (2), one obtains

$$\begin{aligned} t &= \frac{\pi^2\mu L}{\sigma A^2}\left(R_0^4 - R^4\right) + \frac{4\pi^2\mu L}{\sigma A^2}\int_R^{R_0} R'^3\sqrt{1+\gamma_0\frac{R_0}{R'}}\,\mathrm{d}R' \\ &= \frac{\rho}{2\mu L}\left(\frac{\rho\sigma A^2}{8\pi^2\mu^2 L^2}\right)^3\int_{\gamma_0}^{\gamma}\frac{\sqrt{1+\gamma'}+1}{\gamma'^5}\,\mathrm{d}\gamma' \\ &= \frac{\rho R_0^3}{2\mu L}\,\gamma_0^3\int_{\gamma_0}^{\gamma}\frac{\sqrt{1+\gamma'}+1}{\gamma'^5}\,\mathrm{d}\gamma' \end{aligned} \tag{23}$$

Thus, the deflation time becomes

$$\begin{aligned} t_G &= \frac{\pi^2\mu L}{\sigma A^2}R_0^4 + \frac{4\pi^2\mu L}{\sigma A^2}\int_0^{R_0} R'^3\sqrt{1+\gamma_0\frac{R_0}{R'}}\,\mathrm{d}R' = \\ &= \frac{\rho R_0^3}{2\mu L}\,\gamma_0^3\int_{\gamma_0}^{\infty}\frac{\sqrt{1+\gamma'}+1}{\gamma'^5}\,\mathrm{d}\gamma', \end{aligned} \tag{24}$$

where the subscript G refers to the *generalized* case. For clarity, both expressions—with and without γ—have been retained in the equations. As can be seen by inspecting the integral in γ in Eq. (24), if $\gamma_0 \gg 1$ the integrand behaves asymptotically as $\gamma^{-4.5}$ and, consequently, Eq. (24) reduces to Eq. (21). In contrast, if $\gamma_0 \ll 1$, the dominant contribution to the integral comes from the asymptotic limit $2\gamma^{-5}$, which leads t_G to coincide with Eq. (22). This could already be inferred from Eq. (20): for $\gamma \gg 1$, it reduces to the outflow velocity in the inviscid regime, whereas for $\gamma \ll 1$, it corresponds to the velocity in the viscous regime. Referring back to the scenario discussed in Sec. I, and assuming all other parameters remain constant, these two regimes correspond, respectively, to extremely short and extremely long straws.

The expressions in Eqs. (21), (22) and (24) can be rewritten in the following form:

$$\frac{\mu L}{\rho R_0^3}\,t_{\text{deflation}} = \mathcal{H}(\gamma_0), \tag{25}$$

where

$$\mathcal{H}(\gamma_0) = \begin{cases} \dfrac{1}{7\sqrt{\gamma_0}}, & \text{(I)} \\ \dfrac{1}{4\gamma_0}, & \text{(V)} \\ \dfrac{1}{2}\gamma_0^3\displaystyle\int_{\gamma_0}^{\infty}\frac{\sqrt{1+\gamma'}+1}{\gamma'^5}\,\mathrm{d}\gamma', & \text{(G)} \end{cases} \tag{26}$$

is a dimensionless-valued function. This means that the deflation times predicted by the three models can be compared on the same plot without assigning any specific values to the physical parameters μ, σ, and ρ. This analysis will be carried out in the next section.

III. EXPERIMENTAL AND NUMERICAL VALIDATIONS

A. Experimental setup and measurements

In order to determine which of the previous models best describes the deflation process, experimental tests were carried out using the experimental setup shown in Fig. 2. Drinking straws with a cross-sectional area of $16.19\,\mathrm{mm}^2$ and varying lengths were used, along with empty plastic pen refills of $3.14\,\mathrm{mm}^2$ cross-sectional area and 11.2 cm length. A commercially available children's soap solution (97% water and 3% of an unspecified surfactant mixture) produced by the company *Dulcop International* was employed.** Data were collected at 19 °C under dry weather conditions, so it was reasonable to assume $\rho = 1.22(1)\,\mathrm{kg/m}^3$. The remaining quantities, σ and μ, were treated as free parameters in the numerical fits, as their values cannot be precisely determined a priori without appropriate measurement tools, such as a surface tensiometer and a viscometer.

Referring to Fig. 2(a-b), the initial radius of each bubble was set by observing the shadow cast on the paper screen, ensuring that the outermost edges matched the reference length $h = 25.0\,\mathrm{cm}$. The relationship between R_0 and the width of the shadow h is given by

$$R_0 = \frac{d_1\,h}{\sqrt{h^2 + 4\left(d_1+d_2\right)^2}}. \tag{27}$$

Due to the propagation of errors, the uncertainty relative to R_0 is

$$\Delta R_0 = \frac{4d_1\left(d_1+d_2\right)^2\,\Delta h}{\left(h^2+4\left(d_1+d_2\right)^2\right)^{3/2}} + \frac{h\,\Delta d_{1/2}}{\sqrt{h^2+4\left(d_1+d_2\right)^2}}, \tag{28}$$

where Δh and $\Delta d_{1/2} \equiv \Delta d_1 = \Delta d_2$ are the errors on the respective lengths. $\Delta d_{1/2} = 1\,\mathrm{mm}$ due to the scale of the measuring tape, while it is reasonable to assume $\Delta h \approx 2\,\mathrm{mm}$ due to the thickness of the dark edge of the shadow cast on the paper screen. In all experiments, the distances $d_2 = 50.0\,\mathrm{cm}$ and $h = 25.0\,\mathrm{cm}$ were kept fixed, while measurements were taken on bubbles with an initial radius ranging from 2.0 cm to 4.0 cm. As a result, the distance d_1 between the LED and the bubble varied

** Essentially, any commercial bubble solution sold in toy stores is suitable; we simply used the first one we had available.

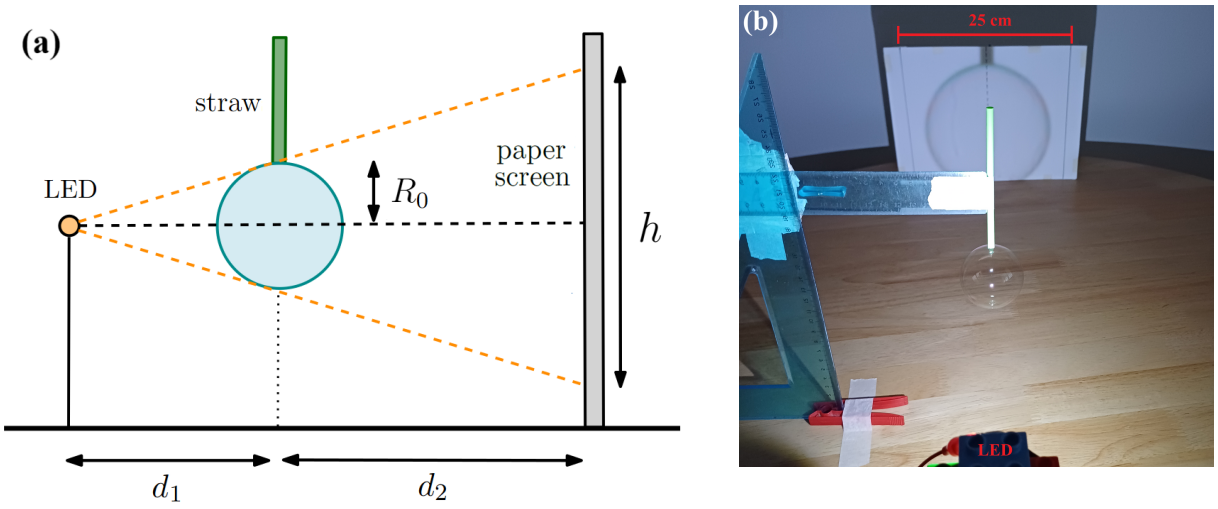

FIG. 2. Experimental setup used for the validation of the theoretical models. The straw was attached to a plastic ruler using ordinary tape. Before each measurement, the lower end of the straw was moistened with the soap solution contained in a plastic cap. Bubbles were inflated by blowing into the upper end of the straw by mouth. The initial radius of each bubble was set by comparing the bubble's shadow—illuminated using an LED—with the reference length drawn on the paper screen. Once the desired value of R_0 was reached, the lips were lifted. From that moment, the deflation time was recorded. Proportions between distances drawn in panel (a) are different in the real configuration, shown in panel (b): they were exaggerated for clarity reasons.

from approximately 10 cm to 24 cm. Consequently, the uncertainty in R_0 ranged between one-third and one-half of a millimeter as given by Eq. (28).

Two types of measurements were conducted. The first involved recording the deflation time with a stopwatch, performing ten measurements for each configuration, and calculating the average times, which are reported in Table I. The second consisted of filming the deflation of bubble with an initial radius of 4.0 cm, attached to a 10.0 cm straw, allowing the experimental function $R(t)$ to be reconstructed using video analysis software. This approach, despite requiring significantly more effort, provided more precise data, enabling the extraction of μ and σ through numerical fits.

Figure 3 shows the comparison among the three models introduced at the end of Sec. II, as a function of the parameter γ_0, together with the experimental data points reported in Table I. It is clearly visible that the experimental points follow the curve corresponding to the generalized model. This result justifies performing a numerical fit of the experimental data based on the generalized model described in Eq. (23), in order to determine the values of the parameters μ and σ. For the same reason, there is no point in performing fits based on the two simpler models.

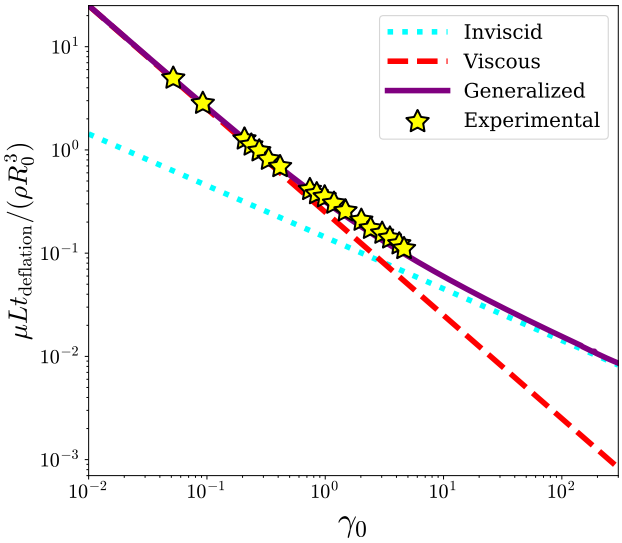

FIG. 3. Comparison of the three models. The experimental data points are taken from the configurations described in Table I. The two measurements related to the empty pen refills are not reported because they are associated with γ_0 values on the order of 10^{-6}.

B. Numerical fit

Six different videos of deflating bubbles with $R_0 = 4.0\,\text{cm}$ and $L = 10.0\,\text{cm}$ were analyzed using Tracker,[9] a video analysis tool that, among other features, can measure instantaneous values of distances in video frames. The yellow star curve in Fig. 4 was obtained by averaging the six sets of data, each consisting of about 55 couples of values $(t_i, R(t_i))$. A numerical fit was performed based on these experimental data, using the least squares method and the generalized model described by Eq. (23), which includes two free parameters,

TABLE I. Data collected from the experiments. Each value in the time column is the average of ten different measurements, with the uncertainty corresponding to the sample standard deviation. The uncertainty in the R_0 values ranges from one-third to half a millimeter, as mentioned in the discussion following Eq. (28).

A (mm^2)	L (cm)	R_0 (cm)	γ_0 (no dim.)	Deflation time (s)
16.19	10.0	4.0	0.74	17.51(25)
		3.5	0.85	10.69(14)
		3.0	0.99	6.28(10)
		2.5	1.19	3.15(6)
		2.0	1.48	1.36(3)
	18.9	4.0	0.21	28.59(28)
		3.5	0.24	16.74(18)
		3.0	0.28	9.26(12)
		2.5	0.33	4.44(8)
		2.0	0.42	1.93(3)
	7.0	3.0	2.02	5.32(8)
		2.5	2.42	2.56(17)
		2.0	3.03	1.18(8)
	5.3	3.0	3.52	4.73(11)
		2.5	4.22	2.40(13)
	28.4	4.0	0.09	42.25(44)
	37.8	4.0	0.05	55.54(52)
	4.0	4.0	4.64	11.73(24)
3.14	11.2	2.5	3.6×10^{-6}	65.71(67)
		2.0	4.5×10^{-6}	26.39(41)

i.e. σ and μ. The fitted parameters are

$$\sigma_G = 0.0248(5)\,\mathrm{kg/s^2}, \quad \mu_G = 1.841(3)\times 10^{-5}\,\mathrm{Pa\cdot s}. \quad (29)$$

The values in Eq. (29) are compatible with those commonly known for soapy water and air at room temperature: the surface tension of typical soapy water is approximately $0.025\,\mathrm{kg/s^2}$,[10] while the viscosity of air lies in the range $(1.78–1.85)\cdot 10^{-5}\,\mathrm{Pa\cdot s}$. From now on, the following set of experimental and fitted parameters

$$R_0 = 4.0\,\mathrm{cm}, \quad L = 10.0\,\mathrm{cm}, \quad A = 16.19\,\mathrm{mm^2},$$
$$\sigma = 2.48\times 10^{-2}\,\mathrm{kg/s^2}, \quad \mu = 1.84\times 10^{-5}\,\mathrm{Pa\cdot s}, \quad (30)$$
$$\rho = 1.22\,\mathrm{kg/m^3},$$

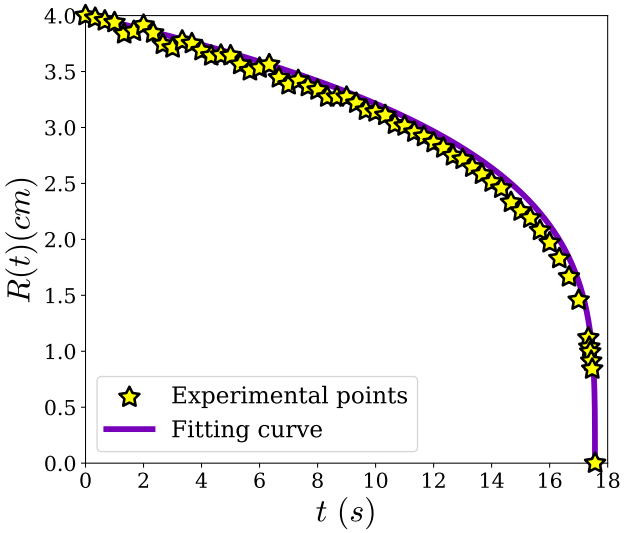

FIG. 4. Experimental curve and numerical fit based on Eq. (23). The initial irregularities of the experimental curve are due to the inevitable oscillations of the bubbles caused by air displaced by the movement of arms.

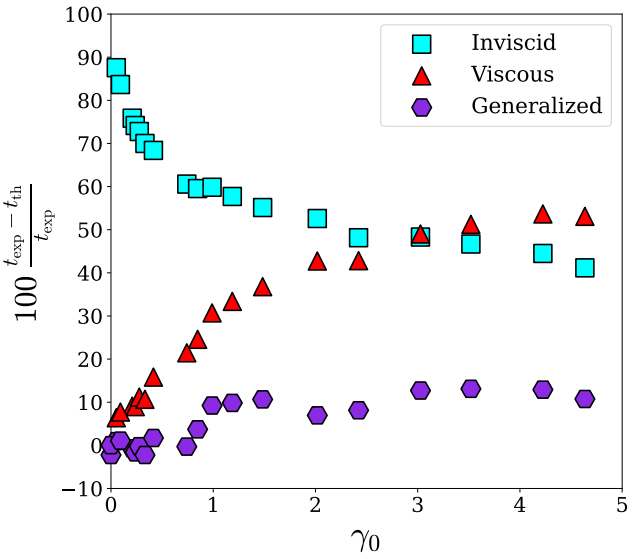

FIG. 5. Percentage difference between measurements and model predictions, as a function of γ_0. The two leftmost data points for the inviscid model error are not shown in the plot, as their values exceed 100. It was not possible to explore values beyond $\gamma_0 = 5$ because the corresponding deflation times drop below one second, making it difficult to perform measurements with an acceptable degree of precision.

corresponding to $\lambda \approx 9\times 10^{-8}\,\mathrm{m}$ and $\gamma_0 \approx 0.74$, will be referred to as the *reference configuration*.

C. Comparison between the models

Using the parameters extracted from the numerical fit in Eq. (29), the theoretical predictions of the three models were compared with the experimental measurements for each configuration listed in Table I. The results of this analysis are shown in Fig. 5, where the percentage differences are plotted as a function of the parameter γ_0. As already seen in Fig. 3, the predictions of the generalized model are noticeably more accurate than those of the simpler models. Moreover, the viscous model provides a very good description of the evolution for $\gamma_0 \ll 1$, but fails outside this regime. In contrast, the inviscid model performs poorly for small values of γ_0, but the relative error decreases as γ_0 increases. However, in all cases, the generalized model consistently outperforms both.

Figure 6 presents a numerical comparison of the inviscid, viscous and generalized model predictions across three regimes, classified according to the value of γ_0. It is evident that for very low values of γ_0, the viscous model offers a good approximation, whereas it fails at higher values—contrary to the inviscid model. In the intermediate regime, however, neither model succeeds in accurately capturing the dynamics of the system. This provides further evidence confirming the superior effectiveness of the generalized model presented in this work.

Finally, a few remarks should be made about the airflow velocity. Since the radius of the bubble tends to zero in the final stages of the process, the theoretical outflow velocity diverges due to the form of the Young–Laplace law, whose denominator approaches zero—this also leads to a divergence in the Reynolds number.[††] However, in the final moments of the process, the bubble can no longer be approximated as a whole sphere. In fact, by examining the final frames in slow motion, it becomes evident that the bubble transforms into an ellipsoidal cap, with its curvature radii never reaching zero.[‡‡] Nevertheless, according to the present modeling, the time spent in the final transient is very short: Eq. (2) implies

$$\mathrm{d}t = -\frac{4\pi R^2(t)}{A\, v_S(t)}\,\mathrm{d}R \equiv f(t)\,|\mathrm{d}R|, \tag{31}$$

where the function $f(t)$ exhibits a sharp decrease in the final stages of the deflation process, due to its numerator approaching zero and its denominator becoming large. In fact, both numerical simulations and experimental results show that the radius goes from $R = 1\,\mathrm{cm}$ to $R = 0$ in approximately one tenth of a second for the reference configuration described in Fig. 4. Thus, the bubble spends only a negligible portion of the total deflation time in the transient phase where $R \sim r_{\mathrm{straw}}$. As a result, the phenomena that cause deviations from the whole-sphere approximation have little impact.

IV. UNSTEADY EFFECTS

So far, steady fluid dynamics equations have been used. Experimental evidence has shown that some models generally fail to describe the phenomenon correctly, such as those based on Eqs. (10) and (14), while the model based on Eq. (17) has succeeded despite the fact that airflow is not strictly steady, either at the beginning or at the end of the deflation process. It is not steady during the first moments because the air outflow velocity goes from zero to a non-zero value given by Eq. (18). As for the final moments, the velocity changes very rapidly because the bubble deflates faster and faster. One might be happy to say that all the approximations made so far are legitimate because the experimental results agree with the model based on the equation, but this is not the case: this section is devoted to mathematically and numerically understanding why the previous approximations are reasonable or not.

When dealing with unsteady flows, Bernoulli's equation must be generalized as described in Ref. 8, 11–16. In the current case, the Unsteady Viscous Bernoulli's Equation (UVBE) connecting quantities inside the bubble to quantities just above the straw reads

$$\rho \int_{\vec{s}_1}^{\vec{s}_4} \frac{\partial \vec{v}}{\partial t}\cdot \mathrm{d}\vec{s} + \frac{1}{2}\rho\left(v_4^2 - v_1^2\right) - \frac{4\sigma}{R(t)} + \frac{8\pi\mu L}{A}\, v_S = 0, \tag{32}$$

where subscripts are relative to the schematization shown in Fig. 1. Assuming that the air velocity inside the bubble is negligible compared to that in the straw, the previous equation becomes

$$\frac{1}{2}\rho v_S^2 - \frac{4\sigma}{R(t)} + \frac{8\pi\mu L}{A}\, v_S \approx -\rho \int_{\mathrm{straw}} \frac{\partial v_S}{\partial t}\,\mathrm{d}s, \tag{33}$$

[††] The Reynolds number associated with the airflow inside the straw/refill is given by $\mathrm{Re} = 2\, v_S\, r_{\mathrm{straw}}\, \rho/\mu$. When the radius of the bubble becomes very small, Re can exceed 2000, indicating a transition to turbulent flow. The main issue with this phenomenon is that it cannot be studied using Bernoulli's equation, not even in its most general form. This is because Bernoulli's theorem relies on the assumption of laminar flow, meaning that streamlines remain smooth and non-intersecting. Turbulence, however, causes streamlines to continuously intertwine and break down over time, making the system inherently unsteady. However, in the configurations analyzed in this work, turbulence is expected to arise when the radius of the bubble reaches a few millimeters, making it even shorter-lived than the unsteady effects that will be discussed in Sec. IV. Consequently, it is not experimentally detectable and does not compromise the overall discussion.

[‡‡] A similar feature is observed in Ref. 2, where bubbles are approximated as spherical caps in the final moments of the process: as they deflate, the radius reaches a minimum before starting to grow again. They do not deform into ellipsoidal caps since they rest on a tube rather than hanging from it, as in the present case. The authors also emphasize the necessity of setting a final radius value to prevent the deflation time from diverging.

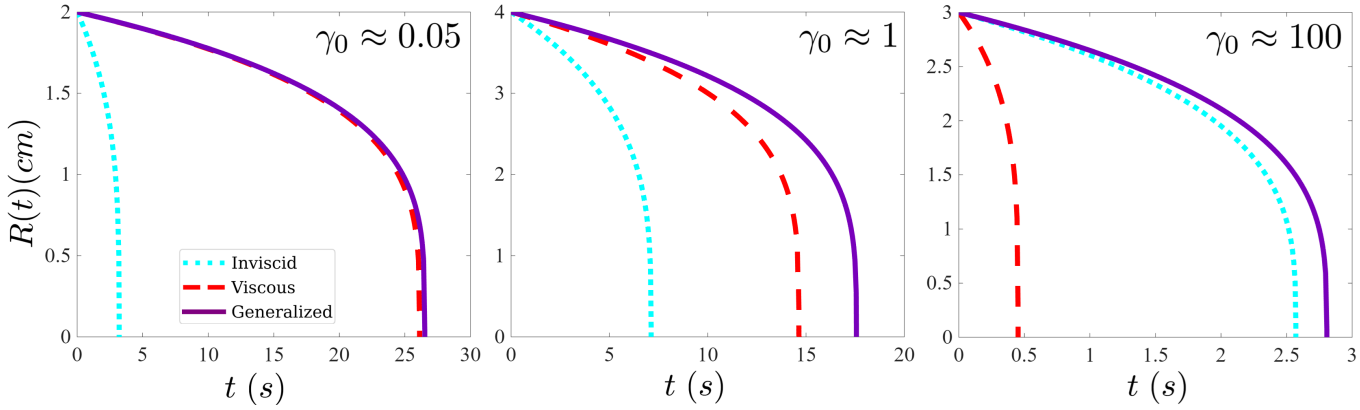

FIG. 6. Comparison between the three models introduced in Sec. II, evaluated for three representative values of γ_0—a small, an intermediate and a large one. *($\gamma_0 \approx 0.05$)* $R_0 = 2\,\mathrm{cm}$, $L = 11\,\mathrm{cm}$, $r_{\mathrm{straw}} = 1\,\mathrm{mm}$; *($\gamma_0 \approx 1$)* $R_0 = 4\,\mathrm{cm}$, $L = 10\,\mathrm{cm}$, $r_{\mathrm{straw}} = 2.45\,\mathrm{mm}$; *($\gamma_0 \approx 100$)* $R_0 = 3\,\mathrm{cm}$, $L = 1\,\mathrm{cm}$, $r_{\mathrm{straw}} = 2.27\,\mathrm{mm}$.

where the last approximation is justified by the fact that the largest contribution in the integral is given by the path inside the straw. Since v_S is homogeneous in the straw, one gets

$$\frac{1}{2}\rho v_S^2(t) - \frac{4\sigma}{R(t)} + \frac{8\pi\mu L}{A}\,v_S(t) = -\rho L\,\frac{\mathrm{d}v_S}{\mathrm{d}t}. \tag{34}$$

A more general version of Eq. (34) can be obtained by taking into account non-zero values of the air velocity inside the bubble. In this case, the evolution of the system is ruled by

$$\begin{aligned}\frac{\rho A}{12\pi R(t)}\frac{\mathrm{d}v_S}{\mathrm{d}t} + \frac{\rho A^2 v_S^2(t)}{96\pi^2 R^4(t)} + \rho L\,\frac{\mathrm{d}v_S}{\mathrm{d}t} \\ + \frac{1}{2}\rho v_S^2(t) - \frac{4\sigma}{R(t)} + \frac{8\pi\mu L}{A}\,v_S(t) = 0,\end{aligned} \tag{35}$$

which is derived in Appendix A using energy considerations. However, for the reference configuration in Eq. (30), numerical calculations show that neglecting the air velocity inside the bubble, i.e. ignoring the first two terms in Eq. (35), yields a difference in the deflation time on the order of one tenth of a millisecond. This was to be expected, since the ratio between the mean kinetic energy densities in the bubble and in the straw is

$$\frac{\frac{1}{2}\rho v_{\mathrm{CM}}^2}{\frac{1}{2}\rho v_S^2} = \frac{\left(\frac{\mathrm{d}R}{\mathrm{d}t}\right)^2}{v_S^2} \overset{\text{Eq. (2)}}{=} \left(\frac{r_{\mathrm{straw}}}{2R}\right)^4, \tag{36}$$

which is on the order of 10^{-5} for most of the duration of the process. Therefore, the assumption of null velocity within the bubble, made in the previous sections, is legitimate. So, it is possible to study the evolution of the system by numerically solving the continuity equation and Eq. (34), with the initial conditions $R(0) = R_0$ and $v_S(0) = 0$.

The solution of Eqs. (2) and (34) corresponds to the green dotted curves in Fig. 7. As shown in Fig. 7(c), the deflation times of the *generalized* and *unsteady* cases differ by approximately 0.07 s, equivalent to a 0.4% variation. This difference is mainly due to the difference in velocity during the initial transient, which is shown in Fig. 7(d). As a result, regardless of the parameter values describing the problem, the steady approximation always underestimates the deflation time compared to the unsteady solution. To better understand such connection, it is possible to obtain an analytical expression for the outflow velocity $v_S(t)$ in the initial transient by replacing $R(t) \to R_0$ in Eq. (34).[§§] This leads to

$$v_S(t) = \sqrt{\left(\frac{8\pi\mu L}{A\rho}\right)^2 + \frac{8\sigma}{\rho R_0}}\,\tanh\left[\tanh^{-1}\left(\frac{2\sqrt{2}\,\pi\mu L}{\sqrt{A^2\rho\sigma/R_0 + 8\pi^2\mu^2 L^2}}\right) + \frac{t}{2L}\sqrt{\left(\frac{8\pi\mu L}{A\rho}\right)^2 + \frac{8\sigma}{\rho R_0}}\right] - \frac{8\pi\mu L}{A\rho}, \tag{37}$$

[§§] Such choice is justified by the following argument. In the first moments of the process, the outflow velocity is really small and the surface of the bubble is the largest. As a consequence, the time derivative of $R(t)$ in Eq. (2) is really small, hence $R(t) \sim R_0$ if $t \ll 1\,\mathrm{s}$.

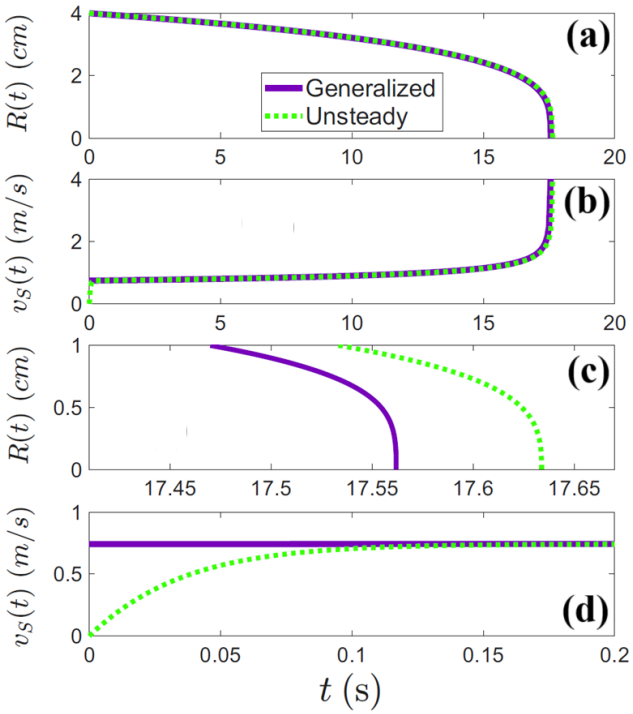

FIG. 7. Comparison between the solution of Eq. (17) (*generalized*) and the solution of Eq. (34) (*unsteady*), in the case of the reference configuration described by Eq. (30). Panels (c) and (d) are zooms of, respectively, panel (a) and (b). As it can be noticed in (d), the outflow velocity in the unsteady case rapidly grows from zero to the value described by Eq. (18), as predicted by Eq. (37).

which corresponds to the dotted green curve in Fig. 7(d). As expected, Eq. (37) tends to Eq. (18) after the unsteady initial transient, whose duration is of the order of the characteristic time

$$\tau = \frac{2L}{\sqrt{\left(\frac{8\pi\mu L}{A\rho}\right)^2 + \frac{8\sigma}{\rho R_0}}} = \frac{A\rho}{4\pi\mu\sqrt{1+\gamma_0}} \approx 0.06\,\mathrm{s} \qquad (38)$$

for the reference configuration in Eq. (30). Further argument for the duration of the initial unsteady transient is given in Appendix B.

Ultimately, unsteady effects can be neglected for all the experimental configurations analyzed in Sec. III, as the initial value of the radius is such that $R \gg r_{\mathrm{straw}}$ for most of the duration of the process. If this were not the case, the green and violet curves in Fig. 7(a-b) would detach, hence unsteady effects should be taken into account. For example, if $R_0 = 1\,\mathrm{cm}$, $L = 10\,\mathrm{cm}$ and $A = 16.2\,\mathrm{mm}^2$, corresponding to $\gamma_0 \approx 2.9$, numerical simulations show that the deflation time of the unsteady solution is about 30% longer than the value obtained using the steady approximation, which yields a duration of approximately 0.1 s. Experimental checks were not performed for such short-duration phenomena, as capturing a sufficient number of frames would require a high-performance camera.

V. CONCLUSION

In conclusion, the new mathematical model proposed based on Eq. (17) proved to be excellent for describing the phenomenon of bubble deflation. This is not true for the simpler models proposed in the literature, which, all parameters being equal, predict shorter deflation times. This difference is far from negligible when, for example, one wants to determine the surface tension of soap with a deflation experiment, as done in Ref. 17. Furthermore, unsteady effects were shown to be irrelevant for bubbles whose initial radius is much larger than the cross-sectional radius of the straw, as for the analyzed experimental configurations.

Appendix A: Unsteady evolution

When some of the hypotheses of Bernoulli's theorem are missing, it is necessary to use one of its generalizations, which has already been discussed in Refs. 11 and 12. For an unsteady, non-turbulent, irrotational flow in an incompressible and viscous fluid, as observed from an inertial frame of reference, it reads

$$\int_{\vec{s}_1}^{\vec{s}_2} \left(\frac{\partial \vec{v}}{\partial t} - \frac{\mu}{\rho}\nabla^2\vec{v}\right)\cdot \mathrm{d}\vec{s} + \left[\frac{p}{\rho} + \frac{1}{2}v^2 + \phi\right]_1^2 = 0, \qquad (A1)$$

where 1 and 2 are two generic points of the fluid. Integrating this equation is a bit messy due to the viscous term. An alternative method to find the equation that describes the evolution of the system involves energy considerations. The balance of energy can be written as

$$\frac{\mathrm{d}W_{\mathrm{ST}}}{\mathrm{d}t} = \frac{\mathrm{d}}{\mathrm{d}t}\left(K_B + K_S\right) + \dot{K}_{\mathrm{out}} + P, \qquad (A2)$$

where W_{ST} is the work done by the surface tension, K_B and K_S are the kinetic energies of the air inside the bubble and in the straw, $\dot{K}_{\mathrm{out}}$ is rate at which kinetic energy exits the straw and P is the power dissipated by viscous forces. Physically speaking, Eq. (A2) means that part of the energy stored on the surface of the bubble becomes kinetic energy, while the remaining part is lost due to viscosity. As the radius of the bubble decreases by a negative amount $\mathrm{d}R$, the work done by the surface tension is

$$\mathrm{d}W_{\mathrm{ST}} = -2\sigma\,\mathrm{d}S = -16\pi\sigma R\,\mathrm{d}R. \qquad (A3)$$

As for the kinetic energy of air inside the bubble, it has been neglected until now. To establish whether such an assumption is reasonable, K_B must be compared to the other terms in Eq. (A2). Given that the airflow in the bubble is not symmetric with respect to its center, it is extremely difficult to exactly evaluate K_B. However, it can be estimated by focusing on the motion of the center of mass. If M is the mass of the air enclosed in the

bubble, then

$$K_B = \frac{1}{2} M v_{\mathrm{CM}}^2 = \frac{2}{3}\,\pi\rho R^3 \left(\frac{\mathrm{d}R}{\mathrm{d}t}\right)^2 = \frac{\rho A^2}{24\pi}\frac{v_S^2}{R}, \tag{A4}$$

where Eq. (2) was used. It should be mentioned that Eq. (A4) loses its validity when $R \sim r_{\mathrm{straw}}$. However, as shown in Sec. III, if $R_0 \gg r_{\mathrm{straw}}$ then the amount of time spent in this stage is negligible compared to the deflation time. The kinetic energy of the air flowing in the straw is

$$K_S = \frac{1}{2}\rho v_S^2 A L, \tag{A5}$$

whereas the rate at which kinetic energy exits the straw is

$$\dot{K}_{\mathrm{out}} = \frac{1}{2}\frac{\mathrm{d}m}{\mathrm{d}t}\, v_S^2 = \frac{1}{2}\rho A v_S^3. \tag{A6}$$

Finally, the expression for the power dissipated by viscous forces in a laminar flow was derived in Ref. 18. In the configuration under exam, it reads

$$P = \mu \int |\nabla v\,|^2 \,\mathrm{d}V, \tag{A7}$$

where the integration is performed over the entire volume of air enclosed in the straw. The velocity of air inside the straw is given by

$$v(r) = \frac{\Delta p}{4\mu L}\left(r_{\mathrm{straw}}^2 - r^2\right), \tag{A8}$$

where r represents the radial coordinate. Performing the integration and exploiting Poiseuille's law, one finds

$$P = 8\pi\mu L v_S^2. \tag{A9}$$

After performing the time derivatives in Eq. (A2), substituting Eq. (2) and dividing the entire equation by $A v_S$, one gets

$$\frac{\rho A}{12\pi R}\left(\frac{\mathrm{d}v_S}{\mathrm{d}t} + \frac{A v_S^2}{8\pi R^3}\right) + \rho L \frac{\mathrm{d}v_S}{\mathrm{d}t} + \frac{1}{2}\rho v_S^2 - \frac{4\sigma}{R} + \frac{8\pi\mu L}{A}\, v_S = 0. \tag{A10}$$

This equation is coupled with Eq. (2): they should be solved simultaneously with appropriate initial conditions to find $R(t)$ and $v_S(t)$.

Appendix B: Duration of the initial transient

Apart from the reasons given in Sec. IV, the steadiness assumption for the initial transient in the viscous case can be justified by the following argument. As shown in Ref. 19, the velocity profile inside the straw at some time t after air starts flowing is

$$v_S(r,t) = \frac{\Delta p}{4\mu L}\left(\frac{A}{\pi} - r^2\right) - \frac{2A\Delta p}{\pi\mu L}\sum_{n=1}^{\infty}\frac{1}{\lambda_n^3}\frac{J_0\left(\lambda_n r\sqrt{\pi/A}\right)}{J_1\left(\lambda_n\right)}\, e^{-\lambda_n^2 \pi\mu\, t/\rho A}, \tag{B1}$$

where J_k are the Bessel functions of the k-th order, λ_n are the positive roots of J_0 and, referring to Fig. 1, $\Delta p \equiv p_3 - p_4 - \rho g L$ (vertical straw). Since the decay time of each term within the sum is $\tau_n \equiv \rho A/\pi\mu\lambda_n^2$,[¶¶] the longest surviving contribution is due to $n = 1$. Since $\lambda_1 \approx 2.4$, the longest decay time is $\tau_1 \approx 0.06\,\mathrm{s}$ for the reference configuration described by Eq. (30), further confirming that the effects due to the initial unsteadiness can be neglected.

ACKNOWLEDGMENTS

The authors thank Nico Kleijne for his suggestions about the numerical fits and all three referees for their helpful comments. Their contribution was very important in improving the quality of this article. D.B.P. expresses gratitude to his lifelong friend Antonino Cilione for producing some nice video simulations of deflating bubbles.

This work served as the theoretical foundation for the final experimental examination of the 2025 Italian Physics Olympiad, annually organized by the Associazione per l'Insegnamento della Fisica (AIF), of which both authors are members.

The authors gratefully acknowledge the Scuola Normale Superiore for supporting the open-access publication of this article.

AUTHOR CONTRIBUTIONS

D.B.P. wrote the drafts and handled the analytical and numerical aspects. The experimental part and data analysis were conducted by A.S.

The core idea of the article was independently conceived by A.S. in 2001 and by D.B.P. in 2024.

CONFLICT OF INTEREST STATEMENT

The authors have no conflicts of interest to disclose.

[1] L. Sibaya, "Time of Collapse of a Soap Bubble," Nature **149**, 527 (1942).

[2] David P. Jackson, Sarah Sleyman, "Analysis of a deflating soap bubble," Am. J. Phys. **78** (10), 990–994 (2010).

[3] Richard Fitzpatrick, *Theoretical Fluid Mechanics* (IOP Publishing, 2017), p. 74-76.

[4] Edgar Buckingham, "On physically similar systems; illustrations of the use of dimensional equations," Physical Review **4** (4), 345-376 (1914).

[5] Lord Rayleigh, "The Principle of Similitude," Nature **95**, 66-68 (1915).

[6] Don S. Lemons, Trevor C. Lipsombe, Rickey J. Faehl, "Vertical quasistatic Poiseuille flow: Theory and experiment," Am. J. Phys. **90** (1), 59–63 (2022).

[7] M. Clerget et al, "Different scenarios of shrinking surface soap bubbles," Am. J. Phys. **89** (3), 244–252 (2021).

[8] Costas Synolakis and Henry Badeer, "On combining the Bernoulli and Poiseuille equation-A plea to authors of college physics texts" Am. J. Phys. **57**, 1013-1019 (1989).

[9] See https://physlets.org/tracker/ for "Tracker".

[10] R. Francisco et al, "A simple experiment for measuring the surface tension of soap solutions," Amer. J. Phys. **69**, 920–921 (2001).

[11] James B. Kelley, "The extended Bernoulli equation," Amer. J. Phys. **18** (4), 202-204 (1950).

[12] Steven B. Segletes and William P. Walters, "A note on the application of the extended Bernoulli equation," International Journal of Impact Engineering **27** (5), 561-576 (2003).

[13] M. Blasone et al, "Discharge time of a cylindrical leaking bucket," Eur. J. Phys. **36** 035017 (2015).

[14] Johann Otto and Carl E. Mungan, "Flow of water out of a funnel," Eur. J. Phys. **45** 055007 (2024).

[15] Johann Otto and Carl E. Mungan, "Filling and emptying a tank of liquid," Eur. J. Phys. **43** 055003 (2022).

[16] Carl E. Mungan and Garth A. Sheldon-Coulson, "Liquid oscillating in a U-tube of variable cross section," Eur. J. Phys. **42** 025008 (2021).

[17] Göran Rämme, "Surface tension from deflating a soap bubble," Phys. Educ. **32**, 191-194 (1997).

[18] Lev D. Landau and E. M. Lifshitz, *Fluid Mechanics: Volume 6* (Pergamon, 2013), p. 54-55.

[19] George K. Batchelor, *An Introduction to Fluid Dynamics* (Cambridge University Press, 1967), p. 193-194.

¶¶ Notice that the decay time does not depend on the length of the tube. This is due to the assumption of incompressible fluid, which lets the propagation of perturbations be instantaneous.